Acta Mech 226, 3807–3822 (2015)
DOI 10.1007/s00707-015-1437-9

ORIGINAL PAPER

M. Şimşek · M. Aydın · H. H. Yurtcu · J. N. Reddy

Size-dependent vibration of a microplate under the action of a moving load based on the modified couple stress theory

Received: 18 February 2015 / Revised: 3 July 2015 / Published online: 8 August 2015

Abstract This study deals with forced vibration analysis of a microplate subjected to a moving load. The formulation is developed based on the modified couple stress theory in conjunction with Kirchhoff–Love plate theory. The equations of motion of the problem are derived using Lagrange's equations. In order to obtain the response of the microplate, the trial function for the dynamic deflection is expressed in the polynomial form. The equations of motion are solved by using the implicit time integration Newmark-β method, and then displacements, velocities and accelerations of the microplate at the considered point and time are determined. Five different sets of boundary condition are considered. For this purpose, boundary conditions are satisfied by adding some auxiliary functions to the trial functions. A parametric study is conducted to study the effects of the material length scale parameter, plate aspect ratio, boundary conditions and the moving load velocity on the dynamic response of the microplate. Also, in order to validate the present formulation and solution method, some comparisons with those available in the literature are performed. Good agreement is found. The results show that the dynamic deflections are significantly affected by the scale parameter and the load velocity.

1 Introduction

Electrostatically actuated microplates can be used as microelectromechanical systems (MEMS) in mass sensing, chemical sensing and signal filtering [1,2]. An electrically driven microplate can be used to form capacitors. These capacitors are used as activators in microsensors, micromirrors, pressure sensors and micropumps [3,4]. Applications of MEMS devices are widely found in chemical, automotive, image processing and biotechnology industries.

M. Şimşek (✉)
Department of Civil Engineering, Faculty of Civil Engineering, Yildiz Technical University, Davutpaşa Campus, 34210 Esenler, Istanbul, Turkey
E-mail: mesutsimsek@gmail.com; msimsek@yildiz.edu.tr
Tel.: +902123835146
Fax: +902123835102

M. Aydın
Department of Mathematics, Faculty of Science and Literature, Yildiz Technical University, Davutpaşa Campus, 34210 Esenler, Istanbul, Turkey

H. H. Yurtcu
Department of Mathematical Engineering, Chemical and Metallurgical Engineering, Yildiz Technical University, Davutpaşa Campus, 34210 Esenler, Istanbul, Turkey

J. N. Reddy
Mechanical Engineering Department, Texas A&M University, College Station, TX 77843-3123, USA
E-mail: jnreddy@tamu.edu

When the thicknesses of the plates and beams are at the microscale or nanoscale, the size effect is observed, as shown experimentally by Lam et al. [5], Chong et al. [6] and Stölken and Evans [7]. Thus, lacking an internal material length scale parameter, classical deformation theories are not capable of calculating the mechanical behavior of micro- and nano-systems. In order to account for scale effects observed at micro- and nanoscale, size-dependent continuum theories have been developed. For example, Mindlin and Tiersten [8], Koiter [9] and Toupin [10] proposed couple stress theory, and Eringen [11] proposed non-local elasticity theory that includes two material length scale parameters. Lam et al. [5] proposed strain gradient theory that includes three material length scale parameters (i.e., l_0, l_1 and l_2).

Determining two or three material length scale parameters is not an easy task so researchers worked to search simpler theories. For this reason, Yang et al. [12] proposed modified couple stress theory in which the couple stress tensor is symmetric and only one internal material length scale parameter is involved in addition to the conventional Lamé's constants. The modified couple stress theory is obtained by letting $l_0 = l_1 = 0$ and $l_2 = l$ in the strain gradient theory of Lam et al. [5]. The material length scale parameter can be determined from torsion tests of slim cylinders of different diameters or bending tests of thin beams of different thickness [13]. By using modified couple stress theory, many works that investigate the static and dynamic analysis of micro-sized and nano-sized beams and plate structures have been done. Akgöz and Civalek [14] used Euler–Bernoulli beam theory to find an analytical solution of the stability problem for axially loaded nano-sized beams based on strain gradient elasticity and modified couple stress theories. Ke and Wang [15] investigated the dynamic stability of microbeams made of functionally graded materials (FGMs) based on the modified couple stress theory and Timoshenko beam theory. Park and Gao [16] developed a new model for the bending of a Bernoulli–Euler beam using modified couple stress theory. Kahrobaiyan et al. [17] employed this model to study the resonant frequency and sensitivity of atomic force microscope (AFM) microcantilevers, and Kong et al. [18] employed this model to solve the dynamic problems of Bernoulli–Euler beams analytically. Ke et al. [19] and Ke and Wang [20] used the Timoshenko beam model to study the vibration of microtubes. Fu and Zhang [21] used this model to study the size effect of microtubules. Xia et al. [22] studied the static bending, postbuckling and free vibration of nonlinear microbeams. Tsiatas [23] developed a new Kirchhoff plate model to analyze the static analysis of isotropic microplates based on a modified couple stress theory. Akgöz and Civalek [24] investigated the free vibration of nanoplates by using the modified couple stress theory. Jomehzadeh et al. [25] applied modified couple stress theory to analyze the vibration of microplates. Ma et al. [26] developed a plate model based on the first-order shear deformation plate theory (FSDT) by using modified couple stress theory that can capture size effects and is sensitive to transverse shear deformation. Roque et al. [27] studied the mechanical behavior of a laminated Timoshenko microbeam by using the meshless method. Chen and Feng [28] compared couple stress theory and strain gradient theory to examine the model of a microcantilever beam bending subject to different loading forms with various material characteristics. Asghari et al. [29] used strain gradient theory to develop a geometrically nonlinear elastic size-dependent Timoshenko beam formulation. Sharafkhani et al. [30] worked on the mechanical behavior of a clamped circular FGM microplate under electrostatic force and mechanical shock. Ke et al. [31] used an FSDT microplate model to study the free vibration of microplates. Roque et al. [32] studied the bending of simply supported micro isotropic plates by using the first-order shear deformation plate theory. Akgöz and Civalek [33] studied the buckling response of size-dependent functionally graded (FG) microbeams for different boundary conditions. Tsiatas and Yiotis [34] studied the static, dynamic and buckling behavior of an orthotropic skew microplate based on the modified couple stress theory using the analog equation method (AEM). Kahrobaiyan et al. [35] established a beam element that recovers the formulations of strain gradient, modified couple stress and classical Timoshenko and Euler–Bernoulli beam elements by using strain gradient theory. Akgöz and Civalek [36] presented a new non-classical sinusoidal plate model on the basis of modified strain gradient theory to investigate bending, buckling and vibration behavior. In addition to the above studies, the modified couple stress theory is also used to study the behavior of microbeams and microplates made of composite materials [37–49].

Moving load problems of beams and plates, which are encountered in many applications (e.g., bridges, guideways and railroads), is one of the major topics of structural engineering. As it is well known, structural members under the action of moving loads produce larger deflections and stresses than they are subjected to an equivalent static load. Due to the importance of this problem, many papers have appeared in the literature. Compared with the problem of beams subjected to moving loads (see [50–68]), the number of studies related to the vibration of plates due to moving loads is rather limited. Gbadeyan and Oni [69] developed a theory related to the response of Rayleigh beams and plates under an arbitrary number of moving masses. Shadnam et al. [70] introduced a new method to compute the transient response of a plate excited by a traveling mass on the surface of a rectangular plate. Kim and McCullough [71] investigated the dynamic displacement and

stress response of a plate on a viscous Winkler foundation under moving in tandem (i.e., axle loads). Lee and Yhim [72] carried out a dynamic analysis of single- and two-span continuous composite plate structures subjected to multi-moving loads. Kim [73] studied the dynamic displacement response of a plate on an elastic foundation. In his study, the system is subjected to in-plane static compressive forces and a moving load with either constant or harmonic amplitude variations. Kim [74] investigated the effect of the horizontal resistance at the plate bottom on the dynamic displacement response of the plate on an elastic foundation when the system is subjected to a moving load with either constant or harmonic amplitude variations. Au and Wang [75] worked on the vibrations of rectangular orthotropic thin plates with general boundary conditions traversed by moving loads. Gbadeyan and Dada [76] analyzed the influence of uniform partially distributed moving loads for Mindlin elastic plates. Wu [77] investigated the dynamic behavior of the inclined plates subjected to moving loads by using the theory for a moving mass element. Malekzadeh et al. [78] studied the dynamic response of cross-ply laminated thick plates subjected to a moving load. Malekzadeh et al. [79] studied the dynamic response of thick laminated annular sector plates with simply supported radial edges subjected to a radially distributed line load. Ghafoori and Asghari [80] studied the dynamic response of angle-ply laminated composite plates due to a moving force. Martinez-Rodrigo and Museros [81] studied the dynamic behavior of orthotropic plates which are simply supported on two opposite sides under the action of moving loads. Vosoughi et al. [82] investigated the dynamic response of moderately thick antisymmetric cross-ply laminated rectangular plates. Malekzadeh and Monajjemzadeh [83] studied the effect of thermal environment on the dynamic response of functionally graded plates under moving loads. Nikkhoo et al. [84] investigated the elastodynamic response of an undamped Kirchhoff plate excited by multiple moving inertial loads.

The above literature review shows that the dynamic analysis of microplates under the action of moving load has not been reported yet. This forms the motivation for the present study. In this paper, a mathematical model is presented for the forced vibration of a microplate under the action of a moving load by using the non-classical Kirchhoff–Love plate theory. An approximate solution is obtained for the considered problem with the help of an energy-based method. The trial function for the dynamic deflection of the microplate is expressed in the polynomial form. The equations of motion are solved by using the implicit time integration Newmark-β method, and then displacements, velocities and accelerations of the microplate at the considered point and time are determined. In the study, five different sets of boundary condition are considered. For this purpose, boundary conditions are satisfied by using the auxiliary functions together with the trial function. The implicit time integration method of Newmark is used to obtain responses in time domain. The influences of the material length scale parameter, aspect ratio, end conditions and the moving load velocity on the dynamic responses of the microplate are examined. Some comparison studies are done to check the validity of the present formulation and solution method. Good agreement is achieved.

2 The modified couple stress theory

Based on the modified couple stress theory, the strain energy of a deformed isotropic linear elastic body can be expressed as [12]

$$U_{\mathrm{s}} = \frac{1}{2}\int_V \left(\sigma_{ij}\varepsilon_{ij} + m_{ij}\chi_{ij}\right) \mathrm{d}V, \quad i, j = x, y, z \tag{1}$$

where U_{s} is the strain energy, σ_{ij} are the components of the classical stress tensor, ε_{ij} are the components of the strain tensor, m_{ij} are the components of the deviatoric part of the couple stress tensor, and χ_{ij} are the components of the symmetric curvature tensor. The components of the strain and curvature tensors can be written as

$$\varepsilon_{ij} = \frac{1}{2}\left(u_{i,j} + u_{j,i}\right), \tag{2}$$

$$\chi_{ij} = \frac{1}{2}\left(\theta_{i,j} + \theta_{j,i}\right), \tag{3}$$

in which u_i are the components of the displacement vector and θ_i are the components of the rotation vector. The rotation vector is given by

$$\theta_i = \frac{1}{2} e_{ijk}\, u_{k,j}. \tag{4}$$

Here, e_{ijk} denotes the permutation tensor. The constitutive relations for an isotropic linear elastic material can be formulated as

$$\sigma_{ij}(x, y, z) = \lambda \varepsilon_{kk} \delta_{ij} + 2\mu \varepsilon_{ij}, \tag{5}$$

$$m_{ij}(x, y, z) = 2\mu l^2 \chi_{ij} \tag{6}$$

where δ_{ij} is the Kronecker delta, l is the material length scale parameter, and λ and μ are Lamé's constants known as

$$\lambda = \frac{E\nu}{(1+\nu)(1-2\nu)}, \quad \mu = \frac{E}{2(1+\nu)} \tag{7}$$

where ν is Poisson's ratio and μ is the shear modulus. It should be noted here that Park and Gao [16] obtained $l = 17.6\,\mu\text{m}$ for epoxy beams by letting $b_h = 17.6\,\mu\text{m}$, $\nu = 0.38$, $l_0 = l_1 = 0$ and $l_2 = l$ in Eq. (68_2) of Lam et al. [5]. Here, b_h is the higher-order bending parameter which characterizes the thickness dependence of beam bending.

3 Non-classical Kirchhoff–Love plate model

A microplate of length a, width b and thickness h is shown Fig. 1. The plate is subjected to a moving load $P(t)$ which moves along the x axis with the constant speed v_P. The following assumptions are made in this study: (i) the microplate is initially at rest, namely the initial conditions are zero; (ii) the velocity of the moving load is constant and the moving load is in contact with the microplate during the excitation; (iii) the inertial effects of the moving harmonic load are negligible; and (iv) the load moves on the x axis.

The displacement components of an initially straight microplate on the basis of Kirchhoff–Love microplate theory can be written as

$$u_x(x, y, z, t) = -z\frac{\partial w_0(x, y, t)}{\partial x}, \tag{8}$$

$$u_y(x, y, z, t) = -z\frac{\partial w_0(x, y, t)}{\partial y}, \tag{9}$$

$$u_z(x, y, z, t) = w_0(x, y, t) \tag{10}$$

where u_x, u_y and u_z are the displacements in x, y and z directions at any material point in the (x, y, z) plane, respectively, w_0 is the transverse displacement, and t denotes time. The kinematic relations produce the following strains:

$$\varepsilon_{xx} = -z\frac{\partial^2 w_0}{\partial x^2}, \quad \varepsilon_{yy} = -z\frac{\partial^2 w_0}{\partial y^2}, \quad \varepsilon_{xy} = -z\frac{\partial^2 w_0}{\partial x \partial y} \tag{11}$$

where ε_{xx} and ε_{yy} are the normal strain and ε_{xy} is the shear strain. By using Eqs. (4), (8–10), the rotation components are found as

$$\theta_x = \frac{\partial w_0}{\partial y}, \quad \theta_y = -\frac{\partial w_0}{\partial x}, \quad \theta_z = 0. \tag{12}$$

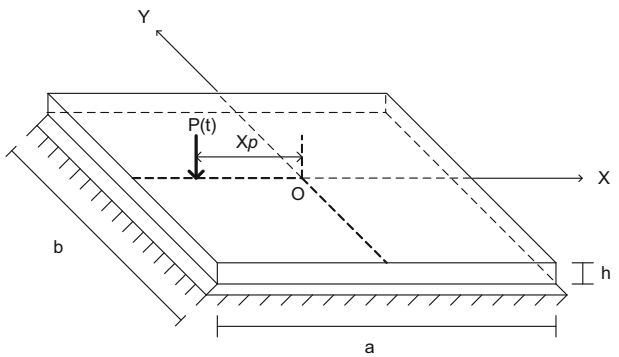

Fig. 1 Microplate subjected to a moving load

If Eq. (12) is put into Eq. (3), the nonzero curvature components can be obtained as

$$\chi_{xx} = \left(\frac{\partial^2 w_0}{\partial x \partial y}\right), \quad \chi_{yy} = \left(-\frac{\partial^2 w_0}{\partial x \partial y}\right), \quad \chi_{xy} = \frac{1}{2}\left(\frac{\partial^2 w_0}{\partial y^2} - \frac{\partial^2 w_0}{\partial x^2}\right), \quad \chi_{xz} = \chi_{yz} = \chi_{zz} = 0. \tag{13}$$

In this study, the equation of motion is derived with the help of Lagrange's equations. Therefore, we need the energy expressions of the microplate. Firstly, the strain energy of the microplate assuming plane stress in the Cartesian coordinates is given by

$$U_{\text{int}} = \frac{1}{2}\int_V \left(\sigma_{xx}\varepsilon_{xx} + \sigma_{yy}\varepsilon_{yy} + 2\sigma_{xy}\varepsilon_{xy} + m_{xx}\chi_{xx} + m_{yy}\chi_{yy} + 2m_{xy}\chi_{xy}\right) \mathrm{d}V. \tag{14}$$

The stress–strain relations for a linear isotropic linear elastic material may be written as

$$\begin{Bmatrix} \sigma_{xx} \\ \sigma_{yy} \\ \sigma_{xy} \end{Bmatrix} = \frac{E}{1-v^2}\begin{bmatrix} 1 & v & 0 \\ v & 1 & 0 \\ 0 & 0 & \frac{1-v}{2} \end{bmatrix} \begin{Bmatrix} \varepsilon_{xx} \\ \varepsilon_{yy} \\ 2\varepsilon_{xy} \end{Bmatrix}, \tag{15}$$

$$m_{ij} = \frac{El^2}{(1+v)}\chi_{ij}. \tag{16}$$

With the help of Eqs. (11) and (13–16), the strain energy of the microplate in terms of displacement can be expressed as

$$U_{\text{int}} = \frac{1}{2}\int_{-a/2}^{+a/2}\int_{-b/2}^{+b/2}\left[(D+S)\left(\frac{\partial^2 w_0}{\partial x^2}\right)^2 + (D+S)\left(\frac{\partial^2 w_0}{\partial y^2}\right)^2 + 2(vD-S)\frac{\partial^2 w_0}{\partial x^2}\frac{\partial^2 w_0}{\partial y^2} + (2D(1-v)+4S)\left(\frac{\partial^2 w_0}{\partial x \partial y}\right)^2\right]\mathrm{d}x\,\mathrm{d}y \tag{17}$$

where

$$D = \frac{Eh^3}{12\left(1-v^2\right)}, \quad S = \frac{Ehl^2}{(1+v)}. \tag{18}$$

The moving load can be expressed as

$$P(x, y, t) = P\delta(x - x_P)\delta(y - y_P), \tag{19}$$

$$x_p = v_P\, t - \frac{a}{2}, \quad -\frac{a}{2} \le x_p(t) \le \frac{a}{2}, \quad 0 \le t \le \frac{a}{v_P}, \quad y_P = 0 \tag{20}$$

where $\delta(\cdot)$ is the Dirac delta function and v_P is the velocity of the moving load. Also, note that $y_P = 0$ since the load moves on the x axis. Thus, the potential energy of the moving load can be written as

$$U_{\text{ext}} = -\int_{-a/2}^{a/2}\int_{-b/2}^{b/2} P(t) w_0(x, y, t)\mathrm{d}x\,\mathrm{d}y. \tag{21}$$

By neglecting the rotary inertia, the kinetic energy of the microplate is given as

$$K_e = \frac{1}{2}\int_{-a/2}^{+a/2}\int_{-b/2}^{+b/2}\rho h\left[\frac{\partial w_0(x, y, t)}{\partial t}\right]^2 \mathrm{d}x\,\mathrm{d}y \tag{22}$$

where ρ is the mass density. It is known that Hamilton's principle can be expressed as Lagrange equations when the functions of infinite dimensions can be expressed in terms of generalized coordinates. Therefore, for applying the Lagrange equations, the displacement function $w_0(x, t)$ is approximated by a series of admissible function that must satisfy the essential (geometric) boundary conditions as follows:

$$w_0(x, y, z, t) = \sum_{m=1}^{N}\sum_{n=1}^{N} A_{mn}(t) G(x, y) x^{m-1} y^{n-1} \tag{23}$$

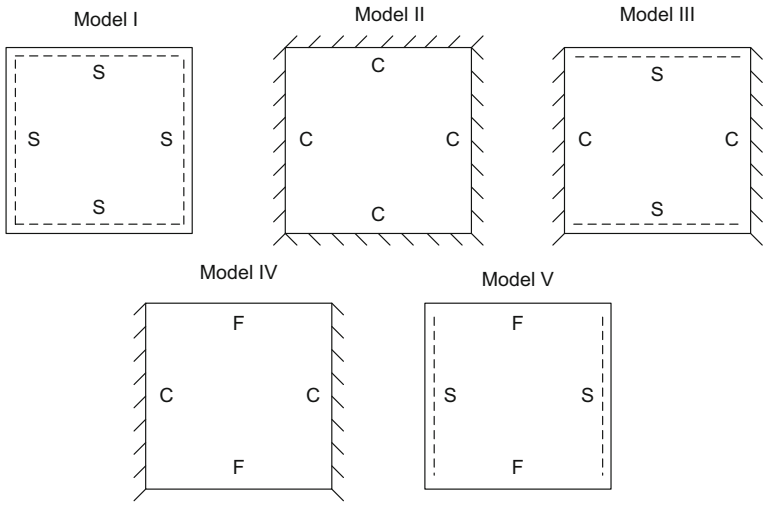

Fig. 2 Microplates with various boundary conditions. *S* simple edge, *C* clamped edge, *F* free edge

Table 1 Different values of the boundary exponents for different plate models

Boundary conditions	p	q	r	s
SSSS	1	1	1	1
CCCC	2	2	2	2
CCSS	2	2	1	1
CCFF	2	2	0	0
SSFF	1	1	0	0

where $A_{mn}(t)$ are the unknown coefficients to be determined and $G(x, y)$ is an auxiliary function which is used to satisfy the geometric boundary conditions. The auxiliary function can be written in the following form:

$$G(x, y) = \left(x + \frac{a}{2}\right)^p \left(x - \frac{a}{2}\right)^q \left(y + \frac{b}{2}\right)^r \left(y - \frac{b}{2}\right)^s \tag{24}$$

where p, q, r and s are the boundary exponents that are related to the boundary conditions. It should be noted that as seen from Fig. 2, five plate models with various boundary conditions are considered in this study. The specific values of the boundary exponents are given for the considered plate models in Table 1.

The equations of motion are derived by using Lagrange's equations which are given as

$$\frac{\mathrm{d}}{\mathrm{d}t}\left(\frac{\partial K_e}{\partial \dot{A}_{kl}}\right) + \frac{\partial U_{\text{int}}}{\partial A_{kl}} + \frac{\partial U_{\text{ext}}}{\partial A_{kl}} = 0 \quad k, l = 1, 2, 3, \ldots, N. \tag{25}$$

Using Lagrange's equations yields the following system of equations of motion:

$$[\mathbf{K}]\{A(t)\} + [\mathbf{M}]\left\{\ddot{A}(\mathbf{t})\right\} = \{\mathbf{F}(\mathbf{t})\} \tag{26}$$

where $[\mathbf{K}]$ is the stiffness matrix, $\{\mathbf{F}(\mathbf{t})\}$ is the time-dependent generalized load vector generated by the concentrated moving load, and $[\mathbf{M}]$ is the mass matrix. The equations of motion are solved by using the implicit time integration method of Newmark-β [85], and then the displacements, velocities and accelerations of the microplate at the considered point and time are determined for any time t between $0 \leq t \leq a/v_P$.

4 Numerical results

In the numerical results, vibration of the microplate made of epoxy due to the moving load is investigated. A comprehensive parametric study is conducted to study the effects of the material length scale parameter, aspect ratio (a/b), boundary conditions and the moving load velocity on the dynamic responses of the microplate. The following parameters are used in the parametric results [39]: $E = 1.44\,\text{GPa}$, $v = 0.38$, $\rho = 1220\,\text{kg/m}^3$, $h =$

88 μm, $b = 10h$. In order to examine the size effect, the plate thickness is kept constant, and the material length scale parameter is computed from various values of l/h ratio, which can be also named as the dimensionless length scale parameter. In the study, five different boundary conditions are considered, such as SSSS, CCCC, CCSS, CCFF and SSFF microplates. In this notation, S, C and F represent the simple, clamped and free edges, respectively. The dynamic deflections are normalized by the static deflection of a square plate under a point load P at the midpoint as given below [86]:

$$w_{\text{st}} = 0.1265\frac{Pb^2}{Eh^3}. \tag{27}$$

The effect of the moving load velocity is reflected by the following dimensionless speed parameter (α)

$$\alpha = \frac{v_P}{v_{\text{cr}}}, \tag{28}$$

$$v_{\text{cr}} = \frac{\omega_{11}a}{\pi}, \tag{29}$$

$$\omega_{11} = \pi^2\left(\frac{1}{a^2} + \frac{1}{b^2}\right)\sqrt{\frac{\bar{D}}{\rho h}} \tag{30}$$

where ω_{11} is the fundamental vibration frequency of the microplate and $\bar{D} = D + S/2$. The dimensionless time t^* is defined by

$$t^* = \frac{x_P}{a} = \frac{v_P\, t}{a} - \frac{1}{2}. \tag{31}$$

It is seen from Eq. (31) that when $t^* = -0.5$ the moving load is at the left edge of the microplate ($x_P = -a/2$), whereas when $t^* = 0.5$ the load is at the right edge of the microplate ($x_P = a/2$). In the numerical analysis, to see the effect of boundary conditions, as given in Table 1, five models with different boundary conditions are considered.

In order to check the present formulation and the numerical results, some comparison effort is presented in this section. In the first example, the deflections of square plates with SSSS, CCCC and SCSC boundary conditions and under the uniformly distributed load are calculated and compared with the available published results. Note that in these calculations the effect of the couple stress is not taken into account for the comparison. For this purpose, the deflection values at the midpoint of the plate by using the present solution technique together with the results of Timoshenko and Woinowsky-Krieger [86] are given in Tables 2, 3 and 4. It is seen from the tables that an excellent agreement is obtained for all boundary conditions.

In order to verify the couple stress formulation, the maximum normalized deflections of an SSSS microplate under sinusoidal load predicted by the present method are compared with the results of Tsiatas [23,43]. By using the numerical data in Refs. [23,43], the deflections at the midpoint of the microplate are calculated for various values of the dimensionless length scale parameter (or l/h ratio) (i.e., $l/h = 0, 0.2, 0.4, 0.6, 0.8, 1$). The comparison given in Table 5 shows that the present results are in good agreement with the results of [23,43].

Table 2 Static deflections at the midpoint of the SSSS plate under uniform load

b/a	Normalized static deflection, $\bar{w} = \frac{10wEh^3}{q_0a^4}$	
	Ref. [86]	Present
1	0.4430	0.4436
1.1	0.5300	0.5316
1.2	0.6160	0.6170
1.3	0.6970	0.6979
1.4	0.7700	0.7734
1.5	0.8430	0.8431
1.6	0.9060	0.9067
1.7	0.9640	0.9644
1.8	1.0170	1.0163
1.9	1.0640	1.0629
2	1.1060	1.1045
3	1.3360	1.3280

Table 3 Static deflections at the midpoint of the CCCC plate under uniform load

b/a	Normalized static deflection, $\bar{w} = \frac{10wEh^3}{q_0a^4}$	
	Ref. [86]	Present
1	0.1380	0.1381
1.1	0.1640	0.1646
1.2	0.1880	0.1882
1.3	0.2090	0.2085
1.4	0.2260	0.2254
1.5	0.2400	0.2392
1.6	0.2510	0.2501
1.7	0.2600	0.2587
1.8	0.2670	0.2651
1.9	0.2720	0.2699
2	0.2770	0.2733

Table 4 Static deflections at the midpoint of the SSCC plate under uniform load

b/a	Normalized static deflection, $\bar{w} = \frac{10wEh^3}{q_0a^4}$	
	Ref. [86]	Present
1	0.2090	0.2094
1.1	0.2740	0.2760
1.2	0.3400	0.3488
1.3	0.4240	0.4253
1.4	0.5020	0.5034
1.5	0.5820	0.5810
1.6	0.6580	0.6566
1.7	0.7300	0.7289
1.8	0.7990	0.7969
1.9	0.8630	0.8602
2	0.9870	0.9184
3	1.2760	1.2537

Table 5 Comparison of the normalized static deflections at the midpoint of the square microplate

l/h	Normalized static deflection, $\bar{w} = \frac{10wEh^3}{q_0a^4}$		
	Ref. [23]	Ref. [43]	Present
0	0.2804	0.2803	0.2802
0.2	0.2401	0.2399	0.2399
0.4	0.1677	0.1676	0.1676
0.6	0.1116	0.1116	0.1115
0.8	0.0760	0.0760	0.0759
1	0.0539	0.0539	0.0538

Table 6 Convergence study for the dimensionless dynamic deflection for $a/b = 1,\ b = 10h,\ h = 88\,\mu\text{m}$

Number of term $N \times N$	l/h	SSSS microplate		CCCC microplate	
		$\alpha = 0.1$	$\alpha = 0.5$	$\alpha = 0.1$	$\alpha = 0.5$
4×4	0	0.9881	1.5321	0.4397	0.6046
6×6		1.0383	1.5739	0.4597	0.6239
8×8		1.0564	1.5759	0.4682	0.6331
10×10		1.0637	1.5751	0.4727	0.6379
4×4	0.5	0.4805	0.7236	0.2166	0.2671
6×6		0.5071	0.7499	0.2266	0.2770
8×8		0.5166	0.7568	0.2309	0.2809
10×10		0.5209	0.7579	0.2331	0.2830
4×4	1	0.1837	0.2759	0.0848	0.0966
6×6		0.1934	0.2859	0.0888	0.1001
8×8		0.1964	0.2897	0.0904	0.1014
10×10		0.1976	0.2911	0.0913	0.1020

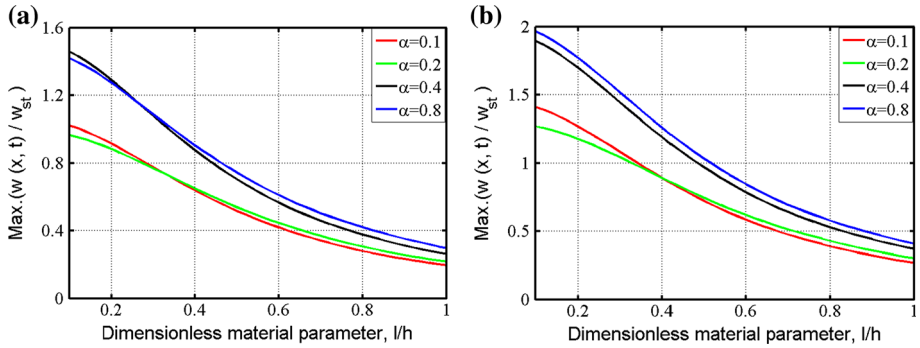

Fig. 3 Variation of the maximum normalized dynamic deflections of an SSSS microplate with *l*/*h* ratio for various velocity parameters (α), **a** $a/b = 1$, **b** $a/b = 2$ ($b = 10h$, $h = 88\,\mu$m)

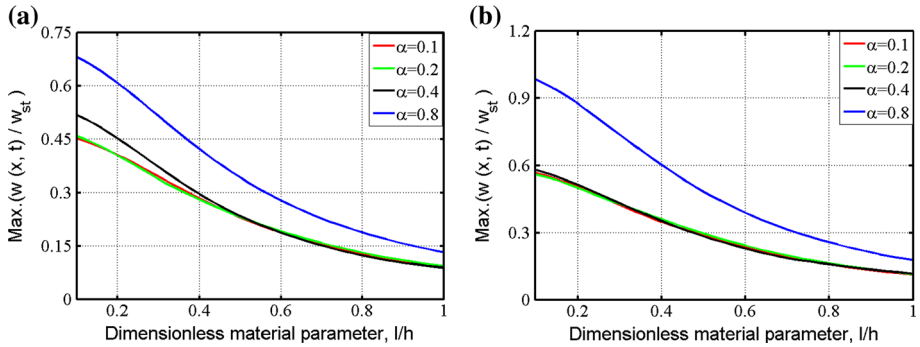

Fig. 4 Variation of the maximum normalized dynamic deflections of a CCCC microplate with *l*/*h* ratio for various velocity parameters (α), **a** $a/b = 1$, **b** $a/b = 2$ ($b = 10h$, $h = 88\,\mu$m)

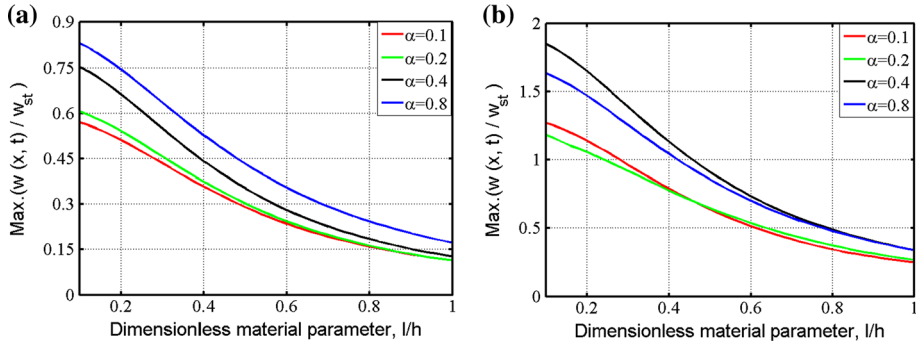

Fig. 5 Variation of the maximum normalized dynamic deflections of a CCSS microplate with *l*/*h* ratio for various velocity parameters (α), **a** $a/b = 1$, **b** $a/b = 2$ ($b = 10h$, $h = 88\,\mu$m)

Before the numerical results, it will be necessary to perform the convergence analysis for the dynamic deflection of the microplate. The convergence study is made for only SSSS and CCCC microplates since the other type of plates gives similar results. For this purpose, the convergence is tested in Table 6 by taking the number of term $N \times N$, where N is taken as 4, 6, 8 and 10. Thus, the size of the corresponding matrices becomes $N^2 \times N^2$ (16×16, 36×36, 64×64, 100×100). Also, it should be noted that the number of the time step is taken as 250 for satisfactory results in the Newmark's procedure. As known, the equations of motion are solved at each time step in the procedure. Thus, the time required for obtaining the solution essentially depends on the number of the term $N \times N$ and time step. For this reason, in order to keep the computational effort reasonable, the number of the terms is taken as 8×8 in the subsequent calculations.

In Figs. 3, 4, 5, 6, and 7, the variation of the maximum normalized deflections of the microplates is presented for different values of the speed parameter ($\alpha = 0.1, 0.2, 0.4, 0.8$). Here, the maximum normalized deflections are calculated at the midpoint of the plates during the traveling of the moving load. Two different aspect ratio

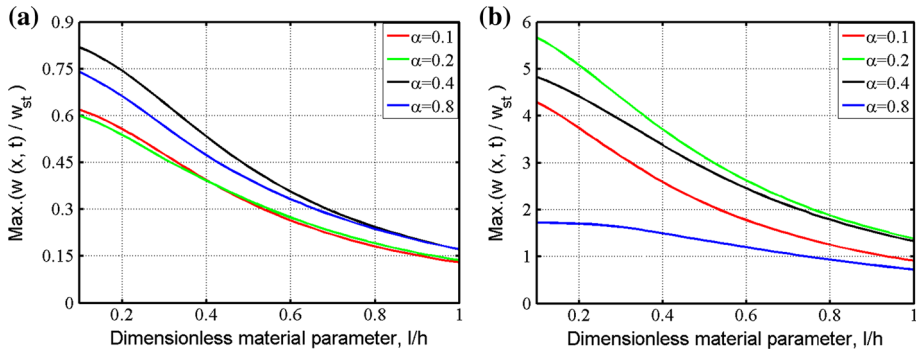

Fig. 6 Variation of the maximum normalized dynamic deflections of a CCFF microplate with l/h ratio for various velocity parameters (α), **a** $a/b = 1$, **b** $a/b = 2$ ($b = 10h$, $h = 88\,\mu\text{m}$)

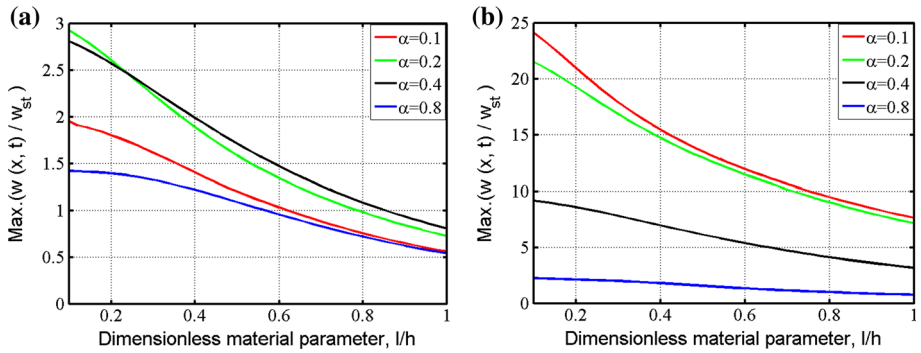

Fig. 7 Variation of the maximum normalized dynamic deflections of an SSFF microplate with l/h ratio for various velocity parameters (α), **a** $a/b = 1$, **b** $a/b = 2$ ($b = 10h$, $h = 88\,\mu\text{m}$)

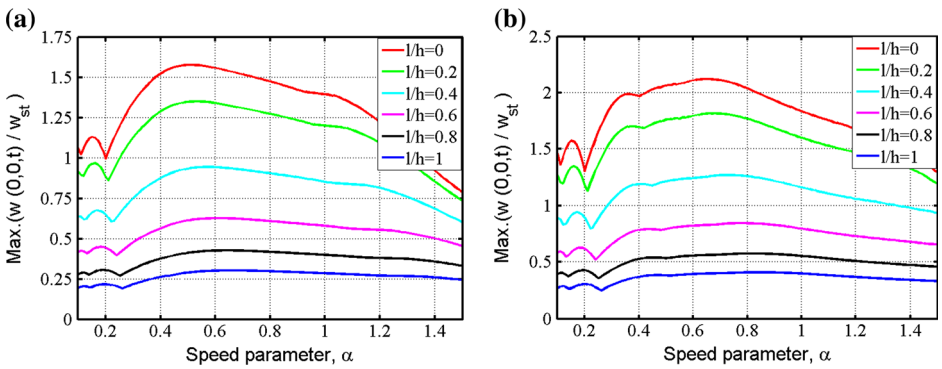

Fig. 8 Variation of the maximum normalized dynamic deflections of an SSSS microplate with the speed parameter for various l/h ratios, **a** $a/b = 1$, **b** $a/b = 2$ ($b = 10h$, $h = 88\,\mu\text{m}$)

values ($a/b = 1, 2$) are considered here. It is seen that while the l/h ratio is increasing, the dimensionless displacements are decreasing. This is because the couple stress is to increase the stiffness of the plate. When the scale parameter is taken zero, namely $l/h = 0$, the results found are the same as the results found with classical plate theory. It can be concluded that the displacements found by the modified couple stress theory are always smaller than the displacements found by the classical theory. As an expected result, the normalized displacements are minimum for a CCCC microplate, whereas they are maximum for an SSFF microplate.

Figures 8, 9, 10, 11 and 12 show the maximum normalized deflections of the microplates versus speed parameter (α) for various values l/h ratio (i.e., $l/h = 0, 0.2, 0.4, 0.6, 0.8, 1$). Also, the same aspect ratio values ($a/b = 1, 2$) are considered here. While establishing these figures, firstly, the maximum deflection at the midpoint of the microplate is determined during the travel of the moving load for each value of the speed parameter. Afterward, the maximum deflections, which are obtained in a similar manner, are plotted

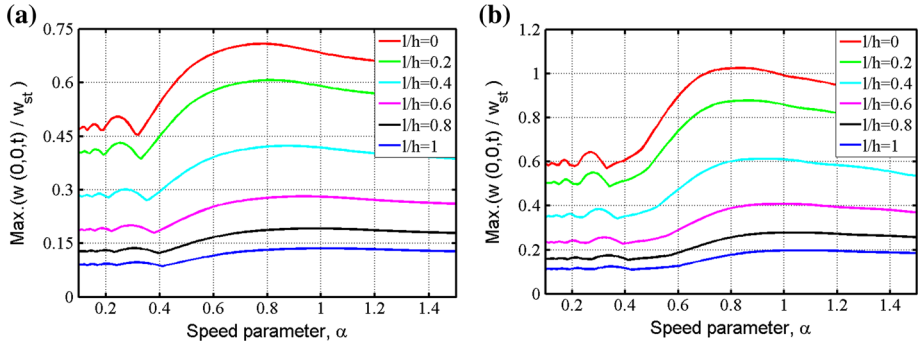

Fig. 9 Variation of the maximum normalized dynamic deflections of a CCCC microplate with the speed parameter for various l/h ratios, **a** $a/b = 1$, **b** $a/b = 2$ ($b = 10h,\ h = 88\,\mu\text{m}$)

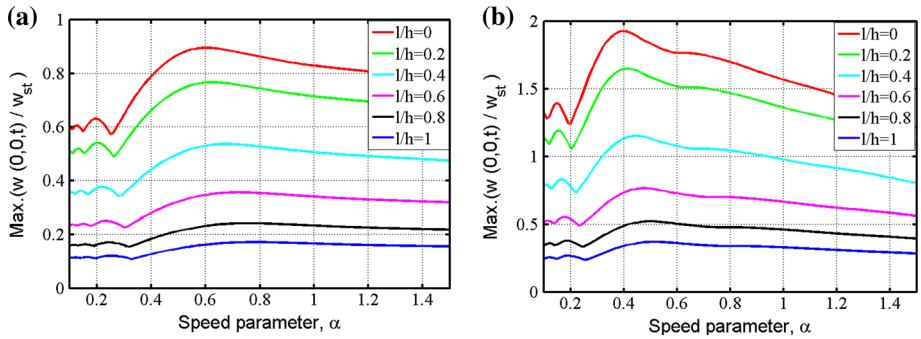

Fig. 10 Variation of the maximum normalized dynamic deflections of a CCSS microplate with the speed parameter for various l/h ratios, **a** $a/b = 1$, **b** $a/b = 2$ ($b = 10h,\ h = 88\,\mu\text{m}$)

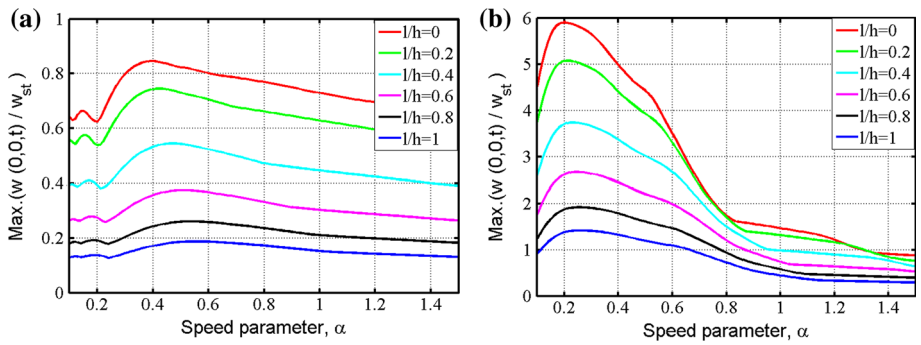

Fig. 11 Variation of the maximum normalized dynamic deflections of a CCFF microplate with the speed parameter for various l/h ratios, **a** $a/b = 1$, **b** $a/b = 2$ ($b = 10h,\ h = 88\,\mu\text{m}$)

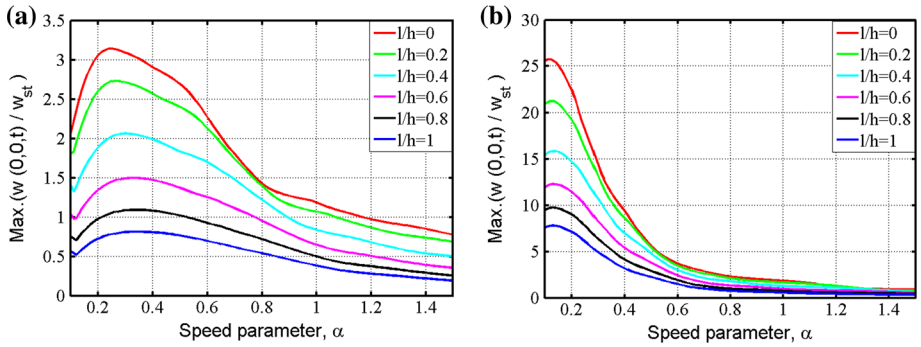

Fig. 12 Variation of the maximum normalized dynamic deflections of an SSFF microplate with the speed parameter for various l/h ratios, **a** $a/b = 1$, **b** $a/b = 2$ ($b = 10h,\ h = 88\,\mu\text{m}$)

Table 7 Maximum non-dimensional dynamic deflections SSSS plate and the corresponding critical velocities for various values of l/h ratio and the aspect ratio, $a/b = 1,\ b = 10h,\ h = 88\,\mu\text{m}$

l/h	a/b	Maximum midpoint deflection, Max. $(w(0, 0, t)/w_{\text{st}})$	Critical speed parameter, α_{cr}
0	1	1.57664	0.51000
0.2		1.34988	0.53000
0.4		0.94297	0.57000
0.6		0.62765	0.61000
0.8		0.42750	0.64000
1		0.30319	0.66000
0	2	2.12077	0.64000
0.2		1.81617	0.66000
0.4		1.26857	0.72000
0.6		0.84418	0.78000
0.8		0.57512	0.82000
1		0.40786	0.84000

Table 8 Maximum non-dimensional dynamic deflections CCCC plate and the corresponding critical velocities for various values of l/h ratio and the aspect ratio, $a/b = 1,\ b = 10h,\ h = 88\,\mu\text{m}$

l/h	a/b	Maximum midpoint deflection, Max. $(w(0, 0, t)/w_{\text{st}})$	Critical speed parameter, α_{cr}
0	1	0.70826	0.78000
0.2		0.60639	0.81000
0.4		0.42358	0.87000
0.6		0.28193	0.93000
0.8		0.19204	0.98000
1		0.13620	1.01000
0	2	1.02657	0.83000
0.2		0.87889	0.87000
0.4		0.61399	0.93000
0.6		0.40868	1.00000
0.8		0.27836	1.05000
1		0.19742	1.08000

Table 9 Maximum non-dimensional dynamic deflections CCSS plate and the corresponding critical velocities for various values of l/h ratio and the aspect ratio, $a/b = 1,\ b = 10h,\ h = 88\,\mu\text{m}$

l/h	a/b	Maximum midpoint deflection, Max. $(w(0, 0, t)/w_{\text{st}})$	Critical speed parameter, α_{cr}
0	1	0.89608	0.60000
0.2		0.76721	0.62000
0.4		0.53595	0.67000
0.6		0.35674	0.72000
0.8		0.24298	0.75000
1		0.17233	0.78000
0	2	1.92528	0.40000
0.2		1.64817	0.41000
0.4		1.15132	0.45000
0.6		0.76634	0.48000
0.8		0.52205	0.50000
1		0.37019	0.52000

as a function of the corresponding speed parameters. The speed parameter (α) is taken into account in the range of $0.1 \leq \alpha \leq 1.5$ with 0.01 increment. As seen from the figures, the maximum normalized deflection increases with the speed parameter until a specific speed parameter; after reaching a peak value, the deflections decrease. The speed parameter corresponding to the peak point of the deflections is named as the critical speed parameter (or critical velocity). In Tables 7, 8, 9, 10 and 11, the maximum value of the maximum normalized deflections and the related critical speed parameters are listed for different values of l/h and aspect ratios. The figures and the tables reveal that the critical speed parameter takes different values depending on the boundary condition. One of the significant results is that for all boundary conditions, while the l/h ratio increases, the critical speed parameter that gives the maximum displacement is increasing. This means that the critical speed

Table 10 Maximum non-dimensional dynamic deflections CCFF plate and the corresponding critical velocities for various values of l/h ratio and the aspect ratio, $a/b = 1,\ b = 10h,\ h = 88\,\mu\text{m}$

l/h	a/b	Maximum midpoint deflection, Max. $(w(0, 0, t)/w_{\text{st}})$	Critical speed parameter, α_{cr}
0	1	0.84591	0.40000
0.2		0.74545	0.42000
0.4		0.54512	0.47000
0.6		0.37511	0.51000
0.8		0.26095	0.54000
1		0.18757	0.56000
0	2	5.91078	0.20000
0.2		5.08379	0.21000
0.4		3.74297	0.23000
0.6		2.67094	0.25000
0.8		1.92374	0.26000
1		1.41958	0.26000

Table 11 Maximum non-dimensional dynamic deflections SSFF plate and the corresponding critical velocities for various values of l/h ratio and the aspect ratio, $a/b = 1,\ b = 10h,\ h = 88\,\mu\text{m}$

l/h	a/b	Maximum midpoint deflection, Max. $(w(0, 0, t)/w_{\text{st}})$	Critical speed parameter, α_{cr}
0	1	3.14207	0.25000
0.2		2.73194	0.27000
0.4		2.06166	0.30000
0.6		1.49874	0.33000
0.8		1.09227	0.34000
1		0.81291	0.34000
0	2	25.74524	0.12000
0.2		21.27855	0.13000
0.4		15.86938	0.13000
0.6		12.31088	0.13000
0.8		9.76586	0.13000
1		7.82100	0.13000

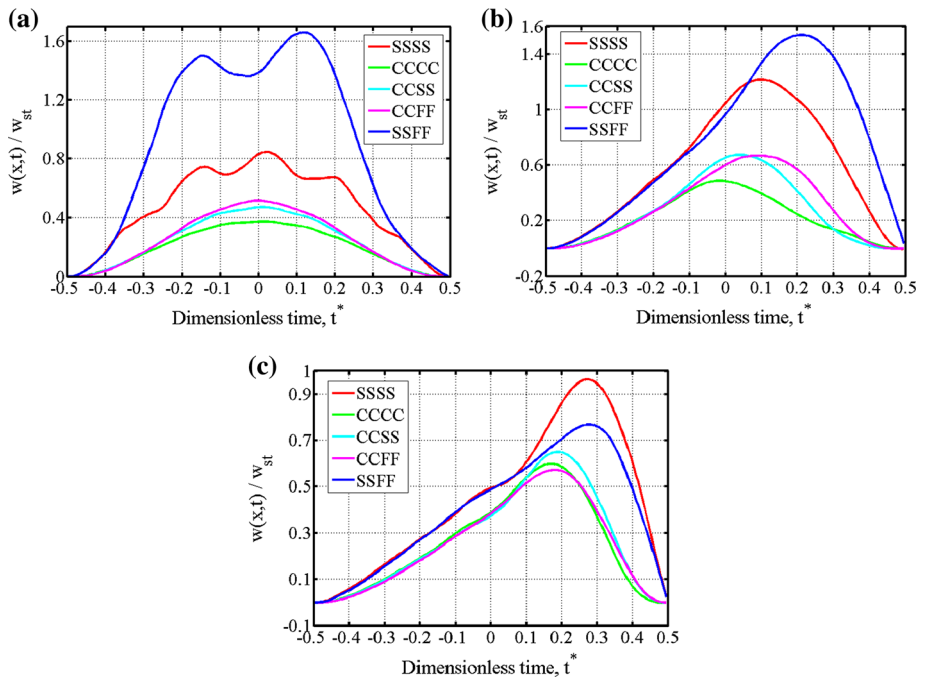

Fig. 13 Time history of the normalized dynamic deflections under the moving load for $l/h = 0.25,\ a/b = 1,\ b = 10h,\ h = 88\,\mu\text{m}$, **a** $\alpha = 0.1$, **b** $\alpha = 0.5$, **c** $\alpha = 1$

parameter increases with the increase in the rigidity of the system. In a similar manner, a CCCC plate, which is the most rigid microplate, has the biggest critical speed parameter. On the other hand, an SSFF plate, which is the least rigid microplate, has the smallest critical speed parameter. It can be generalized from the above results that if the rigidity of the microplate is increased, the critical speed parameter is also increased. It should be noted that regardless of the boundary conditions, while the aspect ratio (a/b) increases, the dimensionless displacements are also increasing.

Figure 13 displays the time history of the dimensionless dynamic deflections of the considered microplates. Here, the dimensionless length scale parameter and the aspect ratio keep constant as $l/h = 0.25$ and $a/b = 1$, respectively, since the other parameters give also similar figures. One can observe from Fig. 13c that for the high value of the speed parameter (i.e., $\alpha = 1$) the dimensionless dynamic deflections under the moving load become smaller than unity. This means that the dynamic deflections are smaller than the static deflections. When the speed parameter increases, the peak point of the deflections shifts toward to the right side of the microplate.

5 Conclusions

In this study, forced vibration of a microplate is investigated within the framework of the size-dependent Kirchhoff–Love plate theory. The Lagrange's equations are applied to obtain the equations of motion. The trial function for the dynamic deflection of the microplate is expressed in polynomial form. The boundary conditions are satisfied by using the auxiliary functions together with the trial function. The implicit time integration method of Newmark is used to obtain responses in time domain. The influences of the material length scale parameter, aspect ratio, support conditions, and the moving load velocity on the dynamic responses of the microplate are examined. Some comparison studies are performed to validate the present results. The comparisons indicate that using the auxiliary functions is a very simple and useful way to satisfy the different combination of end conditions. It is found that the dynamic deflection is very sensitive to the scale parameter and the moving load speed, and the boundary conditions have an important role on the critical speed parameter.

Acknowledgments This study has been supported by The Scientific Research Project Office of Yildiz Technical University with Project No. 2015-05-01-DOP01. This support is gratefully acknowledged.

References

1. Lin, R.M., Wang, W.J.: Structural dynamics of microsystems-current state of research and future directions. Mech. Syst. Signal Process. **20**, 1015–1043 (2006)
2. Batra, R.C., Porfiri, M., Spinello, D.: Review of modeling electrostatically microelectromechanical systems. Smart Mater. Struct. **16**, R23–R31 (2007)
3. Zhang, X.M., Chau, F.S., Quan, C., Lam, Y.L., Liu, A.Q.: A study of the static characteristics of a torsional micromirror. Sens. Actuators A Phys. **90**, 73–81 (2001)
4. Scheeper, P.R., Donk, D., Bergveld, P.: A review of silicon microphones. Sens. Actuators A **44**, 1–11 (1994)
5. Lam, D.C.C., Yang, F., Chong, A.C.M., Wang, J., Tong, P.: Experiments and theory in strain gradient elasticity. J. Mech. Phys. Solids **51**, 1477–1508 (2003)
6. Chong, A.C.M., Yang, F., Lam, D.C.C., Tong, P.: Torsion and bending of micron-scaled structures. J. Mater. Res. **16**, 1052–1058 (2001)
7. Stölken, J.S., Evans, A.G.: A microbend test method for measuring the plasticity length scale. Acta Mater. **46**, 5109–5115 (1998)
8. Mindlin, R.D., Tiersten, H.: Effects of couple-stresses in linear elasticity. Arch. Rat. Mech. Anal. **11**, 415–448 (1962)
9. Koiter, W.T.: Couple stresses in the theory of elasticity, I and II. Nederl. Akad. Wetensch. Proc. Ser. B. **67**, 17–29 (1964)
10. Toupin, R.: Elastic materials with couple-stresses. Arch. Rat. Mech. Anal. **11**, 385–414 (1962)
11. Eringen, A.C.: Nonlocal polar elastic continua. Int. J. Eng. Sci. **10**, 1–16 (1972)
12. Yang, F., Chong, A.C.M., Lam, D.C.C., Tong, P.: Couple stress based strain gradient theory for elasticity. Int. J. Solids Struct. **39**, 2731–2743 (2002)
13. Ma, H.M., Gao, X.L., Reddy, J.N.: A microstructure-dependent Timoshenko beam model based on a modified couple stress theory. J. Mech. Phys. Solids **56**, 3379–3391 (2008)
14. Akgöz, B., Civalek, O.: Strain gradient elasticity and modified couple stress models for buckling analysis of axially loaded micro-scaled beams. Int. J. Eng. Sci. **49**, 1268–1280 (2011)
15. Ke, L.L., Wang, Y.S.: Size effect on dynamic stability of functionally graded microbeams based on a modified couple stress theory. Compos. Struct. **93**, 342–350 (2011)
16. Park, S.K., Gao, X.L.: Bernoulli–Euler beam model based on a modified couple stress theory. J. Micromech. Microeng. **16**, 2355–2359 (2006)

17. Kahrobaiyan, M.H., Asghari, M., Rahaeifard, M., Ahmadian, M.T.: Investigation of the size-dependent dynamic characteristics of atomic force microscope microcantilevers based on the modified couple stress theory. Int. J. Eng. Sci. **48**, 1985–1994 (2010)
18. Kong, S.L., Zhou, S.J., Nie, Z.F., Wang, K.: The size-dependent natural frequency of Bernoulli–Euler micro-beams. Int. J. Eng. Sci. **46**, 427–437 (2008)
19. Ke, L.L., Wang, Y.S., Wang, Z.D.: Thermal effect on free vibration and buckling of size-dependent microbeams. Physica E Low Dimens. Syst. Nanostruct. **43**, 1387–1393 (2011)
20. Ke, L.L., Wang, Y.S.: Flow-induced vibration and instability of embedded double-walled carbon nanotubes based on a modified couple stress theory. Physica E Low Dimens. Syst. Nanostruct. **43**, 1031–1039 (2011)
21. Fu, Y.M., Zhang, J.: Modeling and analysis of microtubules based on a modified couple stress theory. Physica E Low Dimens. Syst. Nanostruct. **42**, 1741–1745 (2010)
22. Xia, W., Wang, L., Yin, L.: Nonlinear non-classical microscale beams: static bending, postbuckling and free vibration. Int. J. Eng. Sci. **48**, 2044–2053 (2010)
23. Tsiatas, G.C.: A new Kirchhoff plate model based on a modified couple stress theory. Int. J. Solids Struct. **46**, 2757–2764 (2009)
24. Akgöz, B., Civalek, O.: Free vibration analysis for single-layered graphene sheets in an elastic matrix via modified couple stress theory. Mater. Des. **42**, 164–171 (2012)
25. Jomehzadeh, E., Noori, H.R., Saidi, A.R.: The size-dependent vibration analysis of micro-plates based on a modified couple stress theory. Physica E Low Dimens. Syst. Nanostruct. **43**, 877–883 (2011)
26. Ma, H.M., Gao, X.L., Reddy, J.N.: A non-classical Mindlin plate model based on a modified couple stress theory. Acta Mech. **220**, 217–235 (2011)
27. Roque, C.M.C., Fidalgo, D.S., Ferreira, A.J.M., Reddy, J.N.: A study of a microstructure-dependent composite laminated Timoshenko beam using a modified couple stress theory and a meshless method. Compos. Struct. **96**, 532–537 (2013)
28. Chen, S.H., Feng, B.: Size effect in micro-scale cantilever beam bending. Acta Mech. **219**, 291–307 (2011)
29. Asghari, M., Kahrobaiyan, M.H., Nikfar, M., Ahmadian, M.T.: A size-dependent nonlinear Timoshenko microbeam model based on the strain gradient theory. Acta Mech. **223**, 1233–1249 (2012)
30. Sharafkhani, N., Rezazadeh, G., Shabani, R.: Study of mechanical behavior of circular FGM micro-plates under nonlinear electrostatic and mechanical shock loadings. Acta Mech. **223**, 579–591 (2012)
31. Ke, L.L., Wang, Y.S., Yang, J., Kitipornchai, S.: Free vibration of size-dependent Mindlin microplates based on the modified couple stress theory. J. Sound Vib. **331**, 94–106 (2012)
32. Roque, C.M.C., Ferreira, A.J.M., Reddy, J.N.: Analysis of Mindlin micro plates with a modified couple stress theory and a meshless method. Appl. Math. Model. **37**, 4626–4633 (2013)
33. Akgöz, B., Civalek, Ö.: Buckling analysis of functionally graded microbeams based on the strain gradient theory. Acta Mech. **224**, 2185–2201 (2013)
34. Tsiatas, G.C., Yiotis, A.J.: Size effect on the static, dynamic and buckling analysis of orthotropic Kirchhoff-type skew micro-plates based on a modified couple stress theory: comparison with the nonlocal elasticity theory. Acta Mech. (2014). doi:10.1007/s00707-014-1249-3
35. Kahrobaiyan, M.H., Asghari, M., Ahmadian, M.T.: A strain gradient Timoshenko beam element: application to MEMS. Acta Mech. **226**, 505–525 (2015)
36. Akgöz, B., Civalek, O.: A microstructure-dependent sinusoidal plate model based on the strain gradient elasticity theory. Acta Mech. **226**, 2277–2294 (2015)
37. Chen, W.J., Li, L., Xu, M.: A modified couple stress model for bending analysis of composite laminated beams with first order shear deformation. Compos. Struct. **93**, 2723–2732 (2011)
38. Ke, L.L., Wang, Y.S., Yang, J., Kitipornchai, S.: Nonlinear free vibration of size-dependent functionally graded microbeams. Int. J. Eng. Sci. **50**, 256–267 (2012)
39. Ke, L.L., Wang, Y.S.: Size effect on dynamic stability of functionally graded microbeams based on a modified couple stress theory. Compos. Struct. **93**, 342–350 (2011)
40. Reddy, J.N.: Microstructure-dependent couple stress theories of functionally graded beams. J. Mech. Phys. Solids **59**, 2382–2399 (2011)
41. Asghari, M., Ahmadian, M.T., Kahrobaiyan, M.H., Rahaeifard, M.: On the size-dependent behavior of functionally graded micro-beams. Mater. Des. **31**, 2324–2329 (2010)
42. Thai, H.T., Choi, D.H.: Size-dependent functionally graded Kirchhoff and Mindlin plate models based on a modified couple stress theory. Compos. Struct. **95**, 142–153 (2013)
43. Thai, H.T., Kim, S.E.: A size-dependent functionally graded Reddy plate model based on a modified couple stress theory. Compos. Part B Eng. **45**, 1636–1645 (2013)
44. Thai, H.T., Vo, T.P.: A size-dependent functionally graded sinusoidal plate model based on a modified couple stress theory. Compos. Struct. **96**, 376–383 (2013)
45. Şimşek, M., Reddy, J.N.: Bending and vibration of functionally graded microbeams using a new higher order beam theory and the modified couple stress theory. Int. J. Eng. Sci. **64**, 37–53 (2013)
46. Şimşek, M., Reddy, J.N.: A unified higher order beam theory for buckling of a functionally graded microbeam embedded in elastic medium using modified couple stress theory. Compos. Struct. **101**, 47–58 (2013)
47. Reddy, J.N., Kim, J.: A nonlinear modified couple stress-based third-order theory of functionally graded plates. Compos. Struct. **94**, 1128–1143 (2012)
48. Gao, X.-L., Huang, J.X., Reddy, J.N.: A non-classical third-order shear deformation plate model based on a modified couple stress theory. Acta Mech. **224**, 2699–2718 (2013)
49. Kim, J., Reddy, J.N.: Analytical solutions for bending, vibration, and buckling of FGM plates using a couple stress-based third-order theory. Compos. Struct. **103**, 86–98 (2013)
50. Fryba, L.: Vibration of Solids and Structures Under Moving Loads. Noordhoff International, Groningen (1972)

51. Lee, H.P.: Dynamic response of a beam with intermediate point constraints subject to a moving load. J. Sound Vib. **171**, 361–368 (1994)
52. Wang, R.T.: Vibration of multi-span Timoshenko beams to a moving force. J. Sound Vib. **207**, 731–742 (1997)
53. Zheng, D.Y., Cheung, Y.K., Au, F.T.K., Cheng, Y.S.: Vibration of multi-span non-uniform beams under moving loads by using modified beam vibration functions. J. Sound Vib. **212**, 455–467 (1998)
54. Zhu, X.Q., Law, S.S.: Moving force identification on multi-span continuous bridge. J. Sound Vib. **228**, 377–396 (1999)
55. Abu-Hilal, M., Mohsen, M.: Vibration of beams with general boundary conditions due to moving harmonic load. J. Sound Vib. **232**, 703–717 (2000)
56. Michaltsos, G.T.: Dynamic behaviour of a single-span beam subjected to loads moving with variable speeds. J. Sound Vib. **258**, 359–372 (2002)
57. Dugush, Y.A., Eisenberger, M.: Vibrations of non-uniform continuous beams under moving loads. J. Sound Vib. **254**, 911–926 (2002)
58. Abu-Hilal, M.: Vibration of beams with general boundary conditions due to a moving random load. Arch. Appl. Mech. **72**, 637–650 (2003)
59. Garinei, A.: Vibrations of simple beam-like modelled bridge under harmonic moving loads. Int. J. Eng. Sci. **44**, 778–787 (2006)
60. Kocatürk, T., Şimşek, M.: Vibration of viscoelastic beams subjected to an eccentric compressive force and a concentrated moving harmonic force. J. Sound Vib. **291**, 302–322 (2006)
61. Kocatürk, T., Şimşek, M.: Dynamic analysis of eccentrically prestressed viscoelastic Timoshenko beams under a moving harmonic load. Comput. Struct. **84**, 2113–2127 (2006)
62. Şimşek, M., Kocatürk, T.: Dynamic analysis of an eccentrically prestressed damped beam under a moving harmonic force using higher order shear deformation theory. ASCE J. Struct. Eng. **133**, 1733–1741 (2007)
63. Şimşek, M., Kocatürk, T.: Nonlinear dynamic analysis of an eccentrically prestressed damped beam under a concentrated moving harmonic load. J. Sound Vib. **320**, 235–253 (2009)
64. Şimşek, M., Kocatürk, T.: Free and forced vibration of a functionally graded beam subjected to a concentrated moving harmonic load. Compos. Struct. **90**, 465–473 (2009)
65. Khalili, S.M.R., Jafari, A.A., Eftekhari, S.A.: A mixed Ritz-DQ method for forced vibration of functionally graded beams carrying moving loads. Compos. Struct. **92**, 2497–2511 (2010)
66. Şimşek, M.: Vibration analysis of a functionally graded beam under a moving mass by using different beam theories. Compos. Struct. **92**, 904–917 (2010)
67. Şimşek, M.: Non-Linear vibration analysis of a functionally graded Timoshenko beam under action of a moving harmonic load. Compos. Struct. **92**, 2532–2546 (2010)
68. Şimşek, M.: Dynamic analysis of an embedded microbeam carrying a moving microparticle based on the modified couple stress theory. Int. J. Eng. Sci. **48**, 1721–1732 (2010)
69. Gbadeyan, J.A., Oni, S.T.: Dynamic behaviour of beams and rectangular plates under moving loads. J. Sound Vib. **182**, 677–695 (1995)
70. Shadnam, M.R., Mofid, M., Akin, J.E.: On the dynamic response of rectangular plate, with moving mass. Thin-Walled Struct. **39**, 797–806 (2001)
71. Kim, S.M., McCullough, B.F.: Dynamic response of plate on viscous Winkler foundation to moving loads of varying amplitude. Eng. Struct. **25**, 1179–1188 (2003)
72. Lee, S.-Y., Yhim, S.-S.: Dynamic analysis of composite plates subjected to multi-moving loads based on a third order theory. Int. J. Solids Struct. **41**, 4457–4472 (2004)
73. Kim, S.M.: Buckling and vibration of a plate on elastic foundation subjected to in-plane compression and moving loads. Int. J. Solids Struct. **41**, 5647–5661 (2004)
74. Kim, S.M.: Influence of horizontal resistance at plate bottom on vibration of plates on elastic foundation under moving loads. Eng. Struct. **26**, 519–529 (2004)
75. Au, F.T.K., Wang, M.F.: Sound radiation from forced vibration of rectangular orthotropic plates under moving loads. J. Sound Vib. **281**, 1057–1075 (2005)
76. Gbadeyan, J.A., Dada, M.S.: Dynamic response of a Mindlin elastic rectangular plate under a distributed moving mass. Int. J. Mech. Sci. **48**, 323–340 (2006)
77. Wu, J.-J.: Vibration analyses of an inclined flat plate subjected to moving loads. J. Sound Vib. **299**, 373–387 (2007)
78. Malekzadeh, P., Fiouz, A.R., Razi, H.: Three-dimensional dynamic analysis of laminated composite plates subjected to moving load. Compos. Struct. **90**, 105–114 (2009)
79. Malekzadeh, P., Haghighi, M.R.G., Gholami, M.: Dynamic response of thick laminated annular sector plates subjected to moving load. Compos. Struct. **92**, 155–163 (2010)
80. Ghafoori, E., Asghari, M.: Dynamic analysis of laminated composite plates traversed by a moving mass based on a first-order theory. Compos. Struct. **92**, 1865–1876 (2010)
81. Martinez-Rodrigo, M.D., Museros, P.: Optimal design of passive viscous dampers for controlling the resonant response of orthotropic plates under high-speed moving loads. J. Sound Vib. **330**, 1328–1351 (2011)
82. Vosoughi, A.R., Malekzadeh, P., Razi, H.: Response of moderately thick laminated composite plates on elastic foundation subjected to moving load. Compos. Struct. **97**, 286–295 (2013)
83. Malekzadeh, P., Monajjemzadeh, S.M.: Dynamic response of functionally graded plates in thermal environment under moving load. Compos. Part B **45**, 1521–1533 (2013)
84. Nikkhoo, A., Hassanabadi, M.E., Azam, S.E., Amiri, J.V.: Vibration of a thin rectangular plate subjected to series of moving inertial loads. Mech. Res. Commun. **55**, 105–113 (2014)
85. Newmark, N.M.: A method of computation for structural dynamics. ASCE Eng. Mech. Div. **85**, 67–94 (1959)
86. Timoshenko, S., Woinowsky-Krieger, S.: Theory of Plates and Shells, 2nd edn. McGraw-Hill Company, New York (1959)